

Measurement of Flux Fluctuations in Diffusion in the Small-Numbers Limit

Effrosyni Seitaridou, Mandar M. Inamdar, and Rob Phillips^{1*}
*Division of Engineering and Applied Science and ¹ Kavli Nanoscience Institute,
 California Institute of Technology, Pasadena, CA 91125*

Kingshuk Ghosh and Ken Dill
Department of Biophysics, University of California, San Francisco, CA
 (Dated: November 6, 2018)

Using a microfluidics device filled with a colloidal suspension of microspheres, we test the laws of diffusion in the limit of small particle numbers. Our focus is not just on average properties such as the mean flux, but rather on the features of the entire distribution of allowed microscopic trajectories that are possible during diffusive dynamics. The experiments show that: (1) the flux distribution is Gaussian; (2) Fick's Law — that the average flux is proportional to the particle gradient — holds even for particle gradients down to one or zero particles; (3) the variance in the flux is proportional to the sum of the particle numbers; and (4) there are backwards flows, where particles flow up a concentration gradient, rather than down it, and their numbers are well-predicted by theory and consistent with a new Flux Fluctuation Theorem.

I. INTRODUCTION

Fick's Law, which describes the diffusion of atoms, molecules, and particles, is important in many areas of science, and is the basis for engineering models of material transport. One statement of Fick's First Law is that the average particle flux is proportional to the average concentration gradient [1],

$$\langle J \rangle = -D \frac{\partial \langle c \rangle}{\partial x}, \quad (1)$$

where $\langle J \rangle$ is the observed macroscopic flux and $\langle c \rangle$ is the concentration of particles. We use brackets here, $\langle \dots \rangle$, to make explicit that this phenomenological expression deals with averages over macroscopically large numbers of particles, and to indicate that the particle concentration and flux can be meaningfully represented as smooth functions of space and time in macroscopic systems. Fick's First Law is the basis for Fick's Second Law, also known as the diffusion equation,

$$\frac{\partial \langle c \rangle}{\partial t} = D \frac{\partial^2 \langle c \rangle}{\partial x^2}. \quad (2)$$

These equations have been extensively verified in bulk gases and solutions with macroscopically large number of particles [2].

Our particular interest here is in the “small numbers” limit of Fick's Law, where there are only a few particles in the system, with special reference to the fluctuations that attend diffusive dynamics. Small particle numbers and their fluctuations are important in nanotechnology; inside biological cells, where the typical copy number of any given type of protein is often less than a few thousand [3]; and in single-molecule studies of ion channels, molecular motors, and in laser trap experiments [4, 5, 6]. Fick's Law describes averages over a macroscopic number of particles; it does not describe small-number fluctuational quantities, such as $\langle J^2 \rangle - \langle J \rangle^2$, or any other aspect of the flux distribution function. One of our motivations for undertaking this work is growing theoretical and experimental interest in nonequilibrium dynamics which centers on the distributions of microtrajectories available to such systems. We reasoned that a first step in examining the distribution of microtrajectories in nonequilibrium systems would be to revisit well-established problems such as diffusion, but with an eye to explicitly measuring (and calculating) the entire distribution of microscopic trajectories.

Does Fick's Law hold in the limit of small numbers of particles? And, are there violations? That is, if Fick's Law predicts flow to the right, due to a concentration gradient sloping downward towards the right, does it ever happen that particles flow instead to the left? Such situations have been called “Second-Law violations” [7, 8]; or, in classical

*Electronic address: phillips@pboc.caltech.edu

thermal problems, they are expressed in terms of “Maxwell’s Demon” [9]. Such fluctuations are, of course, not real violations of the Second Law, because the Second Law is only a statement about averages, not fluctuations [10]. In this article we refer instead to such trajectories that go “against the grain” as *bad-actors*. Our interest here is not just in average fluxes, but in the full flux distribution function. Traditionally, diffusion has been studied in the bulk, where the number of particles is large. Only more recently has it become possible to perform experiments on small-numbers diffusion and on dynamical distribution functions, which explicitly emphasize the character of the microscopic trajectories that describe the dynamics of nonequilibrium systems, based on advances in nanotechnology, video microscopy and microfluidics.

To predict dynamical distributions of diffusion rates, we can use either classical random-flight theory or a recent maximum-entropy-like approach [11], called maximum caliber, based on work of ET Jaynes [12]. In short, if particles are independent, diffusing in one dimension, and if their jump rates are stationary in time, the distribution of particle fluxes, $P(J)$, at time t along an x -axis from one bin at x having N_1 particles, to an adjacent bin at $x + \Delta x$ having N_2 particles, should follow the binomial distribution, or approximately a Gaussian function [11],

$$\begin{aligned} P(J) &= \frac{1}{\sqrt{2\pi\langle(\Delta J)^2\rangle}} \exp\left(-\frac{(J - \langle J \rangle)^2}{2\langle(\Delta J)^2\rangle}\right) \\ &= \frac{1}{\sqrt{2\pi(pqN)}} \exp\left(-\frac{(J - p\Delta N)^2}{2pqN}\right), \end{aligned} \quad (3)$$

where $\Delta N = N_1 - N_2$, $N = N_1 + N_2$, $\langle\Delta J^2\rangle$ is the variance in the flux J , and $q = 1 - p$, with p being the probability that a particle jumps in the time interval Δt .

Various moments of the distribution function are readily obtained from this model. First, the model predicts that the average net number of particles, J , that jump per unit time at time t is [11]

$$\langle J \rangle = \langle j_1 - j_2 \rangle = -\frac{p}{\Delta t} \Delta N, \quad (4)$$

where j_1 is the flux from the bin 1 at x to bin 2 at $x + \Delta x$, and j_2 is from bin 2 to 1. This proportionality of the average flux $\langle J \rangle$ to ΔN , simply predicts Fick’s Law, where the diffusion coefficient D is related to p by $D = p\Delta x^2/\Delta t$, and where Δx is the bin size and Δt is the unit time step.

For the flux fluctuations, i.e., the second moment, the model predicts

$$\langle\Delta J^2\rangle = \langle(J - \langle J \rangle)^2\rangle = \frac{p(1-p)}{\Delta t^2} N, \quad (5)$$

where $N = N_1 + N_2$ is the total number of particles associated with the two bins of interest. Hence, the key prediction here is that the flux fluctuations are proportional to the total particle number, N .

We are also interested in the number of *bad-actors*, i.e., the number of trajectories that would lead to particle flows up a concentration gradient, rather than down it. This quantity can be derived from the flux distribution [11] as

$$\begin{aligned} \Phi_{\text{badactors}} &= \frac{1}{2} \left(1 - \text{erf} \left(\frac{\langle J \rangle}{\sqrt{2\langle(\Delta J)^2\rangle}} \right) \right) \\ &\approx \frac{1}{2} - \frac{1}{\sqrt{2\pi}} \frac{\langle J \rangle}{\sqrt{\langle(\Delta J)^2\rangle}} \cdots \\ &\quad + \mathcal{O} \left\{ \left(\frac{\langle J \rangle}{\sqrt{\langle(\Delta J)^2\rangle}} \right)^3 \right\}, \end{aligned} \quad (6)$$

where the approximation holds for small values of $\langle J \rangle / \sqrt{\langle(\Delta J)^2\rangle}$. In the expression above, the next higher term (the cubic term), is an order of magnitude smaller than the linear term for the values of $\langle J \rangle / \sqrt{\langle(\Delta J)^2\rangle}$ used in our experiments (see Figure 3).

A. A “Flux” Fluctuation Theorem

Recently, a useful description of nonequilibrium dynamics has involved fluctuation theorems. Fluctuation theorems characterize the extent to which the system deviates from its dominant flow behavior [8, 13, 14, 15, 16]. In the

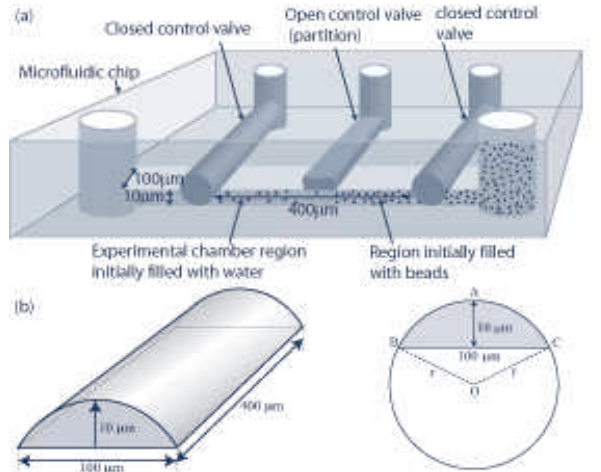


FIG. 1: The microfluidics experiment. Colloids corralled on one side of a gate begin to diffuse at time $t = 0$ by opening the gate. (a) Schematic of the microfluidic chip (see text for details). (b) The geometry of the microfluidic chamber (not drawn to scale).

diffusive dynamics case of interest here, if the number of particles N_1 in bin 1 is greater than the number of particles N_2 in bin 2, then particles, on average, will flow from 1 to 2. Fluctuation theorems describe the amount of reverse flow. Ours is a *flux* fluctuation theorem, i.e., it is expressed in terms of the quantity $P(J)/P(-J)$, where J is the flux. This differs from fluctuation theorems [8, 13] expressed in terms of entropies, $P(\Delta S)/P(-\Delta S)$ and from the work theorems of Jarzynski and Crooks, which are expressed in terms of the work w as $P[w/(kT)]/P[-w/(kT)]$ [17]. In our approach, the ratio $P(J)/P(-J)$, obtained from Eq. 3, gives the ratio of probabilities of fluxes in the forward and backward directions [11],

$$\ln \frac{P(J)}{P(-J)} = \frac{2\langle J \rangle}{\langle (\Delta J)^2 \rangle} J. \quad (7)$$

Thus, the quantity $\ln[P(J)/P(-J)]$ is predicted to be proportional to the normalized flux $\langle J \rangle / \langle (\Delta J)^2 \rangle \times J$. In situations having large flux, the back-flow becomes exponentially negligible. We subjected these predictions to experimental tests.

II. THE MICROFLUIDICS EXPERIMENTS

To study the dynamical distributions in diffusion, we devised a microfluidics experiment. Using the techniques of soft lithography, chip fabrication [18] and the Sylgard 184 Silicone elastomer kit (Dow Corning Corporation), we made a microfluidics chamber having approximate dimensions $400\mu\text{m}$ by $100\mu\text{m}$, partitioned into two regions (see Fig. 1a). The cross-section of this chamber is a segment of a circular disc, with a maximum depth of $10\mu\text{m}$ (see Fig. 1b). The chamber is filled on one side with a solution containing about 200 colloidal, green fluorescent polystyrene particles $0.29\mu\text{m}$ in diameter (Duke Scientific, Cat. No. G300) (see Fig. 1a). The beads are at an optimized concentration so that the interactions are negligible [19] while at the same time permitting sufficient statistics over a wider range of ΔN and N .

At time $t = 0$, we open a microfluidic gate, allowing particles to diffuse from one side to the other, and we begin taking periodic snapshots under an Olympus IX71 inverted microscope. (We performed the same experiment under equilibrium conditions where the initial concentration was uniform across the whole chamber (results not shown, see [20])). We take 3 snapshots of the beads in the chamber every time interval of $\Delta t = 10$ seconds for 6 hours. Since there is a possibility that within one snapshot some particles are temporarily overlapping and/or are out of focus, the 3 snapshots are used to minimize that error. The snapshots are taken using fluorescence microscopy with a SONY DFW-V500 camera. (During the time when no snapshots are taken, a shutter prevents the experimental chamber from being exposed to the incident light, to prevent photobleaching and heating the chamber.) We then determine the particle positions at each snapshot using a computerized centroid tracking algorithm [25]. The time-dependent particle density is determined by dividing the chamber into a number of equal-sized bins of value Δx each along the longest dimension of $400\mu\text{m}$ and by computing the number of particles in each bin as a function of time.

Although the microfluidic chamber is three-dimensional, it can be shown that, in the case of weak particle-particle and particle-wall interactions, the problem can be collapsed to a one-dimension diffusion problem. Therefore, we bin only along the x-axis, the direction of the concentration gradient. The choice of the bin size will affect the statistics for each combination of N_1 and N_2 as well as the range of N and ΔN themselves. If the bin size is too big, then there will not be enough statistics and, in addition, the range of values for N will not include small numbers (since it will be rare to have 1 or 2 particles in a single bin). On the other hand, if the bin size is too small, we may not have a sufficient range of values for N and ΔN (since it will be rare to have more than a couple of particles in the small bin). Also, in this case, there will be an increased probability for a particle to have multiple jumps across bins within the time interval Δt . Therefore, the optimal choice of the bin size was made based on the bead's expected mean excursion within the time-interval Δt , which is $\sqrt{2D\Delta t}$. This is the only relevant microscopic length scale. Here, D is the diffusion coefficient for an individual bead given by the Stokes's formula [26]. For a bead of $0.29\mu\text{m}$ in diameter suspended in water at room temperature, the Stokes's formula gives a diffusion coefficient D of approximately $1.5\mu\text{m}^2/\text{second}$. This value, within experimental error, is equal to the one we obtain by fitting our data of the concentration profile at different times to the one dimensional diffusion equation using D as our fitting parameter (i.e. $D = 1.3 \pm 0.27\mu\text{m}^2/\text{second}$). This gives a bin size of $\Delta x \approx 5\mu\text{m}$. By observing all the consecutive bin pairs for all the frames taken we were able to obtain, on average, about 5000 points for each combination of N_1 and N_2 . Given the bead concentration in the microfluidics channel, the N_1 and N_2 ranged from 0 through 6. The choice of bin size determines the value of the jump probability p , as discussed in [21].

We can find the flux at a plane i at a specific time interval from the computed particle distribution statistics as a function of position x and time t mentioned above. Since the microfluidic chamber is isolated, the total number of particles stays the same from one frame to the next. As a result of this conservation in particle number, the flux at plane $i + 1$ (J_{i+1}), i.e., the plane that separates bins i and $i + 1$, can be easily evaluated by using the continuity equation,

$$N_i(t + \Delta t) = N_i(t) + (J_i(t) - J_{i+1}(t)) \Delta t \quad (8)$$

$$\Rightarrow J_{i+1}(t) = -\frac{N_i(t + \Delta t) - N_i(t)}{\Delta t} + J_i(t), \quad (9)$$

where N_i is the number of particles in bin i . Since the microfluidic chamber is isolated, from our boundary conditions the flux J_0 (flux at $x = 0$) is zero at all times. Combined with Eq. 9, we obtain $J_1(t)$. Thus, from the analysis of these images, we obtain complete sets of the values of $\{N_i(t)\}$ and $\{J_i(t)\}$ in all the bins and at all times of observation. Then, for each pair of consecutive bins with specific values of N_1 and N_2 , we construct the histogram of J values. Upon normalization the histogram becomes the flux probability distribution, $P(J)$.

III. RESULTS

A. The Flux Distribution Function is Gaussian.

Figure 2 shows our observed particle flux distribution function at the optimized concentration. All the data falls on a single master curve where $\langle J \rangle$ and $\langle (\Delta J)^2 \rangle$ have been calculated separately from each combination of N_1 and N_2 . The quadratic form observed on this log plot shows that the distribution function is Gaussian. The theory predicts that: (i) the coefficient of the square term should be -1 , (ii) the coefficient of the linear term should be zero, and (iii) the constant term should be $\ln(\Delta J_{\text{bin}}/\sqrt{2\pi}) \approx -0.9$, where ΔJ_{bin} is the bin-size used to obtain the histogram and is equal to 0.1second^{-1} , i.e., 1 particle per unit time. Consistent with these predictions, the coefficient observed for the square term is -0.98 , for the linear term is -0.0018 , and for the constant term is -0.94 . The coefficient of determination for the quadratic fit is $R^2 = 0.98$. Next, we analyze the bad actors – the backward flows – in two different ways.

B. The Bad-Actor Trajectory Counts are Well Predicted by the Model.

Equation 6 predicts that, for small values of $\langle J \rangle / \sqrt{\langle (\Delta J)^2 \rangle}$, the fraction of bad-actors should be linearly proportional to $\langle J \rangle / \sqrt{\langle (\Delta J)^2 \rangle}$. In good agreement, Figure 3 confirms this linearity and gives the predicted intercept of 0.5. This means that as the system approaches equilibrium (i.e. $\langle J \rangle \approx 0$), about half the trajectories involve flow down the vanishingly small gradient and half the trajectories involve flow up that small gradient. In the linear regime, the best fit line shows the slope to be 0.37, which agrees well with the expected value of $1/\sqrt{2\pi} \approx 0.4$ from Eq. 6. The coefficient of determination for the linear fit is $R^2 = 0.99$. Another key feature of this graph is that when the system

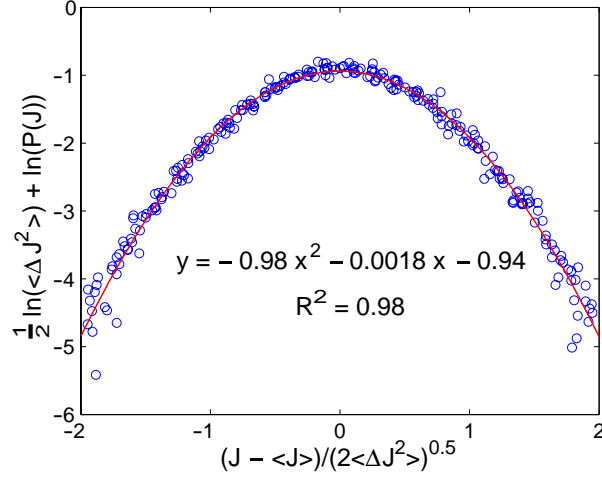


FIG. 2: The flux distribution function. $\frac{1}{2} \ln(\langle \Delta J^2 \rangle) + \ln(P(J))$ is plotted against $(J - \langle J \rangle) / \sqrt{2\langle \Delta J^2 \rangle}$, based on the form indicated by Equation 3. Circles indicate experimental points, the line shows a quadratic fit to the data. The coefficient of determination (R^2) for the fit is also reported. This demonstrates that the distribution function is Gaussian, and we find that the coefficients are well predicted by Equation 3.

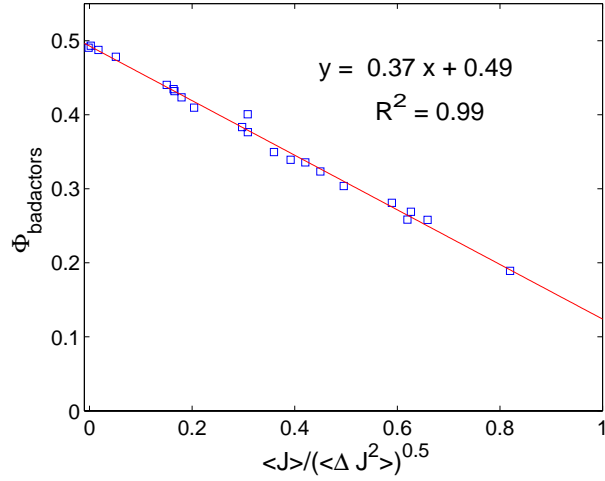


FIG. 3: The fraction of trajectories that are bad-actors vs. the deviation from equilibrium as characterized by the normalized mean flux, $\langle J \rangle / \sqrt{\langle \Delta J^2 \rangle}$. Experimental data is shown in squares, while the solid line represents the fit to the data. The coefficient of determination (R^2) for the fit is also reported. The slope and intercept agree well with the model.

is farther away from equilibrium (as implied by a larger mean flux), the bad-actor fraction reduces. What this means is that more of the microtrajectories available to the system in this case are potent to change the current state of the system. Indeed, in our earlier paper we characterized this idea quantitatively in the form of the potency [11].

C. The Experiments Confirm the Flux Fluctuation Theorem.

Figure 4 shows $\ln(P(J)/P(-J))$ vs. the flux, normalized by $\langle J \rangle J / \langle \Delta J^2 \rangle$, to account for different averages and variances of the flux distribution. This rescaling leads to a linear master curve as predicted by Eq. 7. Experiments show the slope to be 2.0, in perfect agreement with the predicted slope of 2 from Eq. 7. In this figure, there are a few aberrant data points that we are unable to explain. However, the coefficient of determination is still close to unity, $R^2 = 0.77$. Though ultimately the fluctuation theorem is a reflection of the nature of the flux distribution function, such theorems are a compact way to quantitatively illustrate the significance of bad-actor microtrajectories.

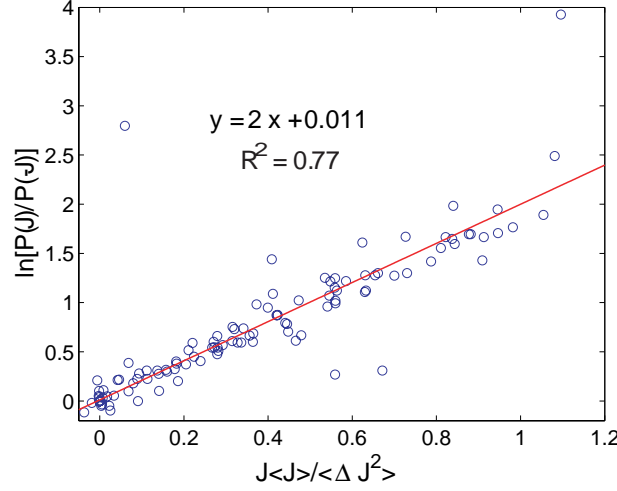


FIG. 4: The flux fluctuation theorem. The plot shows $\ln[P(J)/P(-J)]$ vs. $\langle J \rangle J / \langle (\Delta J)^2 \rangle$ for different values of $\langle J \rangle$ and $\langle (\Delta J)^2 \rangle$ arising due to different combinations of N_1 and N_2 . Experimental data is shown in circles, while the solid line represents the fit to the data. The coefficient of determination (R^2) for the fit is also reported. The slope and intercept agree with the prediction of Equation 7.

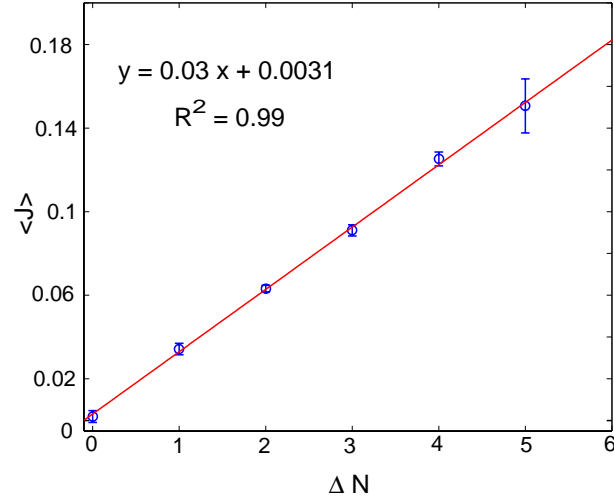


FIG. 5: Experimental support for Fick's Law, even down to few-particle gradients. The average flux, $\langle J \rangle$, is shown as a function of ΔN , the gradient in the particle number between two neighboring bins. Experimental data is shown in circles, while the solid line represents the fit to the data. The coefficient of determination (R^2) for the fit is also reported. The error bars shown are the variances due to the different combinations of N_1 and N_2 resulting in the same ΔN . The slope and intercept are in agreement with the expected theoretical values, based on Equation 4.

D. Fick's Law Holds Even in the Small-Numbers Limit.

We compare the average flux between two neighboring bins, $\langle J \rangle$, with the difference in particle numbers, $\Delta N = N_1 - N_2$. This data is compiled from all the values of N_1 and N_2 that provide a given ΔN . Fig. 5 shows that $\langle J \rangle$ depends linearly on the particle number gradient ΔN , even down to “gradients” of zero or one particle, indicating that Fick's Law holds in the small-numbers limit. The slope of the graph (0.03/second) also gives us a value of the jump rate, $p = 0.3$, which is in good agreement with the theoretical estimate of 0.33 made in terms of the bin-size and the diffusion coefficient [21]. As expected, the intercept is close to 0 (see Equation 4). The linear fit has a coefficient of determination $R^2 = 0.99$.

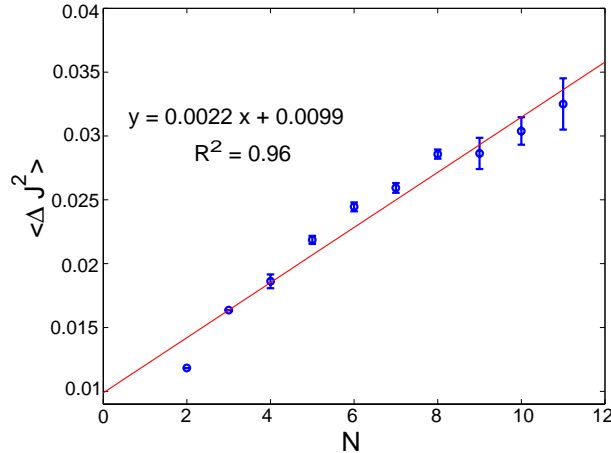


FIG. 6: The second cumulant, $\langle \Delta J^2 \rangle = \langle J^2 \rangle - \langle J \rangle^2$, vs. the total number of particles, N . The second moment of particle flux is proportional to the sum of particle numbers in the two bins. Experimental data is shown in circles, while the solid line represents the fit to the data. The coefficient of determination (R^2) for the fit is also reported. The error bars show the variances due to the different combinations of N_1 and N_2 that result in the same N . The slope and intercept are well predicted by Equation 5.

E. The Second Moment of Particle Flux is Proportional to the Sum of Particle Numbers.

Equation 5 predicts that the second moment of the flux should be proportional to the sum of particle numbers in the two bins, $N = N_1 + N_2$. Figure 6 confirms this dependence of $\langle \Delta J^2 \rangle = \langle (J - \langle J \rangle)^2 \rangle$ on N . For the optimized particle concentrations, the slope (0.0022/second²) is equal to the expected slope of 0.0022/second² for the value of $p = 0.33$. The coefficient of determination is $R^2 = 0.96$. At higher particle concentrations (data not shown), however, not surprisingly, systematic errors begin to appear and the slope deviation is quite high compared to the expected value. We performed Brownian dynamics simulations that show the likely cause of these concentration-dependent errors is non-conservation of bin counts, from particles that either overlap or go out of focus in one snapshot and into focus in the next (see previous section).

IV. CONCLUSIONS

In a microfluidics experiment, we have determined the distribution of particle fluxes in few-particle diffusion. Random-flight and maximum-caliber models predict a gaussian distribution of fluxes. Moreover, with a single parameter p , which is essentially the diffusion constant, we find agreement of the theory with several experimental properties which are usually not examined in diffusion, and are in direct analogy with quantities of recent interest in other nonequilibrium experiments [8, 14, 15, 16]. First, we find that Fick's law – the proportionality of average flux to the gradient of average concentration – holds even down to concentration gradients as small as a single particle. Experiments also confirm that the variance in the flux is proportional to the total number of particles, $\langle J^2 \rangle \propto N_1 + N_2$, with correct slopes within experimental errors. In addition, we describe a new “flux fluctuation theorem”, that is found to be consistent with the data in predicting an exponentially diminishing number of variant trajectories, as a function of the deviation from equilibrium. The model predicts the backwards flows, the bad actors, which are relatively infrequent situations in which particles flow up — rather than down — their concentration gradients and shows that this subset of the overall repertoire of microscopic trajectories can be characterized quantitatively.

V. ACKNOWLEDGEMENTS

We thank S. Blumberg, F. Brown, D. Drabold, P. Grayson, L. Han, C. Jarzynski, J. Kondev, H. J. Lee, H. Qian, S. Quake, S. Ramaswamy, U. Seifert, T. Squires, Z.G. Wang, E. Weeks, and D. Weitz for helpful and stimulating comments and discussions. K.A.D. and M.M.I. would like to acknowledge support from NIH Grant No. R01GM034993, E.S. acknowledges support from the Betty and Gordon Moore Fellowship, and R.P. acknowledges support from NSF

Grant No. CMS-0301657, CIMMS, the Keck Foundation, NSF NIRT Grant No. CMS-0404031, and NIH Director's Pioneer Award Grant No. DP1 OD000217.

-
- [1] Dill, K.; Bromberg, S. *Molecular driving forces: statistical thermodynamics in chemistry and biology*; Garland Sciences: New York, 2003
 - [2] Baker, R.W. *Controlled release of biologically active agents*; Wiley: New York, 1987
 - [3] Wu, J-Q; Pollard, T.D. *Science* **2005**, **310** (5746), 310
 - [4] Hille, B. *Ion channels of excitable membranes*; Sinauer Associates 2001
 - [5] Howard, J. *Mechanics of motor proteins and the cytoskeleton*; Sinauer Associates Inc. 2001
 - [6] Neuman, K.C. and Block, S. M. *Rev. Sci. Inst.* **2004**, **75**, 2787
 - [7] Evans, D.J.; Cohen, E.G.D. and Morriss, G.P. *Phys. Rev. Lett.* **1993**, **71**(15), 2401.
 - [8] Evans, D.J.; Searles, D.J. *Adv. Phys.* **2002**, **51**, 1529.
 - [9] Feynman, R. *Feynman lectures on computation*; Preseus, 1996
 - [10] Callen, H.B. *Thermodynamics and an introduction to thermostatics*; Wiley, 1985.
 - [11] Ghosh, K.; Dill, K.; Inamdar, M.; Seitaridou, E; Phillips, R. *Am. J. Phys.* **2006**, **74**, 123.
 - [12] Jaynes, E.T. *E. T. Jaynes: Papers on probability, statistics and statistical physics*; Kluwer academic publishers, 1980.
 - [13] Crooks, G.E. *Phys. Rev. E* **1999**, **60**, 2721.
 - [14] Blickle, V.; Speck, T.; Helden, L.; Seifert, U.; Bechinger, C. *Phys. Rev. Lett.* **2006**, **96**, 070603.
 - [15] Collin, D.; Ritort, F.; Jarzynski, C.; Smith, S.; Tinoco, I.; Bustamante, C. *Nature* **2005** **437**, 231.
 - [16] Feitosa, K.; Menon, N. *Phys. Rev. Lett.* **2004**, **94**, 164301.
 - [17] Crooks G. *Ph.D. Thesis* **1999**
 - [18] Unger, M. A.; Chou, H.P.; Thorsen, T.; Scherer, A.; Quake, S.R. *Science* **2000**, **288**, 113.
 - [19] The bead concentration is such that the mean particle spacing is about $8\mu\text{m}$. For such large particle separations, electrostatic [22] and hydrodynamic interactions [23, 24] are negligible. Although the polystyrene particles have a small negative surface charge, it is readily shown using the Poisson-Boltzmann equation that there is little interaction at these separations, and we confirmed that result by an experiment showing an independence on salt concentrations (data not shown). Also, the data of Meiners and Quake [23] and Dufresne *et al.* [24], applied to our system, show that hydrodynamic interactions should be small.
 - [20] The results obtained under the equilibrium setting were similar to the ones presented in this paper. However, the equilibrium measurements were not presented since the local concentration gradient was obviously rather small, thus limiting the range of ΔN values.
 - [21] The jump probability p in the time interval Δt from bin $i - 1$ to bin i (of size Δx) can be estimated from the diffusion of a particle with diffusion coefficient D . However, there is also a possibility of a jump occurring from any of the other bins to bin i . After summing all the jump probabilities from all the neighboring bins, the effective probability p is found to be $p \simeq 0.33$, for the given values of Δx and Δt and D .
 - [22] Crocker, J.C.; Grier, D.G. *Phys. Rev. Lett.* **1994**, **73**, 352.
 - [23] Meiners, J-C.; Quake, S.R. *Phys. Rev. Lett.* **1999**, **82**, 2211.
 - [24] Dufresne, E.R.; Squires, T.M.; Brenner, M.P.; Grier, D.G. *Phys. Rev. Lett.* **2000**, **85**, 3317.
 - [25] Crocker, J.C.; Grier, D.G. *J. Coll. Int. Sci.* **1996** **179** 298.
 - [26] Reif, F. *Fundamentals of statistical and thermal physics*; McGraw-Hill; New York 1965.